Nigerian Journal of Materials Science and Engineering

Volume 10 Issue 1 May 2020

Nigerian Journal Of Materials Science and Engineering (NJMSE)

Volume 10 Issue 1 ISSN 214-453-2 May 2020

Materials Science & Technology Society of Nigeria (MSN)

An International Journal of the Materials Science and Technology Society of Nigeria

Nigerian Journal of

Materials Science and Engineering

(NJMSE)

Materials Science & Technology Society of Nigeria (MSN)

Volume 10 Issue 1, May 2020
ISSN 214-453-2

Published by

Materials Science and Technology Society of Nigeria (MSN)
National Headquarters
Engineering Materials Development Institute (EMDI)
Km. 4 Ondo Road,
P. M. B. 611, Akure. Nigeria
Tel.: +234-803-471-8487; +234-803-703-3052; +234-806-220-7420

http://njmse.msn.ng
NJMSE@msn.ng; njmse.msn@gmail.com; editorinchief@msn.ng; njmsemanagingeditor@msn.ng; bbabatop@oauife.edu.ng;giwafat2002@yahoo.com

(NJMSE - An International Journal of the Materials Science and Technology Society of Nigeria)

NJMSE Editorial Board

Editorial Comment

It is a great pressure for the editorial board of the Nigerian Journal of Materials Science and Engineering (NJMSE) to present Volume 10 Number 1 of the journal for 2020 for the world research and development community.

The Materials Science and Technology Society of Nigeria (MSN), as a professional learned body, has made the publication of this research journal to be of very good quality and high standard comparable to any in her class. Our major thrust is to disseminate materials science and engineering and allied research activities from Nigeria, Africa and the world over. We are slowly and gradually impacting on the research community work with this specialised journal from a reputable learned and professional body in Nigeria. We are presently not insisting on number but we very much believe, with the thoroughness of our approach to the review and assessment process, we are convinced that with our resolve to publish quarterly, the board is convinced that more researcher would take advantage of this.

As a journal whose policy is to maintain the standard best practices and in addition to help young researchers to advance in the art and science of scientific findings dissemination, had faced tremendous challenges which were expected. It is heart-warming that we can look back and be glad to see the society publishing the 10th volume. These volumes and the previous ones would be available for FREE downloading on our society website (www.msn.ng) through a link prior to the specialised journal website to be available soon. Arrangements are in advanced stages for the hosting of this journal by reputable international online submission system are being worked on.

Volume 10 (2020) Number 1 consists of eight (8) high standard articles covering different specialised areas of materials research. It is our hope that this humble effort, presently by voluntary efforts of senior members of the Society, at disseminating research findings as put together in this volume which have contributed to the body of knowledge, would have enriched the information base and complemented Materials Research efforts from around the world.

We appreciate all our reviewers and associate editors involved for their prompt action on the manuscripts and cooperation as we look forward to submission of manuscripts which can be forwarded as detailed below.

Babaniyi Babatope. (PhD,MBA,FMSN,FIMMM(UK))
Editor-in-Chief.
Department of Physics and Engineering Physics,
Advanced Nanostructured Materials and Devices Research Group
Obafemi Awolowo University, Ile-Ife. Nigeria.
bbabatop@oauife.edu.ng
editorinchief@msn.ng; njmse.editor.in.chief@gmail.com.

Manuscripts can also be submitted and copied to:

Managing Editors, NJMSE.
njmsemanagingeditor@msn.ng; njmse.msn@gmail.com; njmse@msn.ng.

Editor-in-Chief
editorinchief@msn.ng;njmse.editor.in.chief@gmail.com

Website:
http://njmse.msn.ng/

GUIDE TO AUTHORS

AIM: *T*o improve the international exchange of scientific research in materials science and engineering.

INTRODUCTION

The Nigerian Journal of Materials Science and Engineering (NJMSE) publishes reviews, full-length papers, and short communications recording original research results on, or techniques for studying the relationship between structure, properties, and uses of materials. The subjects are seen from international and interdisciplinary perspectives covering areas including metals, ceramics, glasses, polymers, composite materials, fibers, electronic materials, alternative energy materials, nanostructured materials, nanocomposites, biological, biomedical materials, etc. The NJMSE is now firmly established as the leading source of primary communication for scientists investigating the structure and properties of all engineering materials in Nigeria, Africa and the Rest of the World.

UNIQUENESS OF THE JOURNAL

NJMSE is introduced to publish research findings on current topical issues of interest to both public and private sectors. The scope of the Journal focuses on experimental, empirical and theoretical research in Materials Science and Engineering. Findings from multidisciplinary research covering diverse areas of interest with potential impact on the public and private sectors of both the national and international communities will be priorities of the journal. Our major focus is the use of Materials Science and Engineering principles to solve basic problems peculiar to African and the developing world while contributing to knowledge on the global scale.

GUIDE FOR AUTHORS

NJMSE welcomes research papers covering original work that has good potential for practical application. Submission of a manuscript will be held to imply that the work being reported is original and that the result has not been published previously nor been under considerations for publication elsewhere.

MANUSCRIPT PREPARATION

The format of the typescript should be as follows:

The official language of the journal is English. When writing do not mix languages, use US English completely or use UK English completely. It is expected that before submission, the manuscript will have been thoroughly reviewed and written in simple clear expression. Manuscript should be typewritten with double-spacing and 2.54 cm or 1 inch margins on all sides. Manuscripts should be submitted in electronic form and e-mailed directly to the addresses below in MS-Word format, double spacing with graphics at the end. Manuscripts should be arranged in the following order: title page, abstract, introduction, materials and methods, results and discussion, conclusions, acknowledgements, references. The manuscripts should follow the format listed below.

Title: The title page should contain the title [concise but clear expression, written in bold, upper case], followed by the authors [surname first, block letters throughout], and followed by their institutional affiliations and the e-mail address of the corresponding author. In case of many authors, please use numbers to differential their affiliation.

Abstract: An abstract of not more than 350 words should be supplied immediately before the beginning of the paper (Graphical abstracts are also acceptable).

Introduction: This should contain a brief review of literature, clearly stated objectives and justification for the study.

Materials and Methods: This should contain materials preparation procedure and major measurement patterns. Sufficient information should be provided to perform repetition of the experimental work.

Results and Discussion: The result section should contain appropriate tables, figures/illustrations**.** These should be pertinent to the work and should clearly indicate the degree of reliability of results. Tables should be numbered consecutively, with a short descriptive title in upper case (block letters) on top of the table. They should contain no vertical lines and no lines to separate the rows except the heading and the end of the table. Figures, micrographs, or illustrations must be clearly captioned, the captions at the bottom of each figure. Figures may not be used to repeat the information already presented in tables or text or vice versa. Micrographs and illustrations are considered as figures and must be labeled as such.

Conclusions: These should summarize any important conclusions emerging from the work.

Acknowledgements: These should be presented at the end of text and before the references. Technical assistance and advice may be acknowledged. Acknowledgments of financial support can also be stated in this section.

References:

Citing: Reference in the text should be made by the author's last name and year of publication, e.g. (Abel, 2007); (Abel and Babcock, 2007); (Bowen *et al*., 2007). Two papers by the same author in the same year should be distinguished by a suffix, (a, b, etc) e.g. (Madonna, 2006a); (Madonna, 2006b).

Listing: This should be in alphabetical order and should follow this format: Name(s) and initial(s) of author(s), (year of publication), exact title of paper (in quote), the title of periodical, Vol. (number)**:** initial and final page numbers. Please note that only name cited in the text can be used.

Serial: Briant C. L. and Banerji S. K. (1981). Tempered Martensite Embrittlement and Intergranular Fracture in an Ultrahigh Strength Sulfur Doped Steel, *Metall. Trans. A,* 12A:309-319. (Please pay attention to punctuations).

Book: Samuels, L.E. (1982). *Metallographic Polishing by Mechanical Methods,* 3ed., American Society for Metals, Metals, Park, Ohio.

Proceeding: Olorunnisola A. O. (2006). The potentials of bamboo as novel building and furniture production materials in Nigeria, pp.180-185. In *Proc. Nigerian Materials Congress (NIMACON 2006),* (B. Babatope and W.O. Siyanbola, Eds.), organized by Materials Society of Nigeria, 15-18 November 2006, Abuja, Nigeria.

Heading and sub-heading: All headings and sub-headings should be numbered and started from the left hand margin. All headings should be in upper case while sub-headings should be in lower case except the first letter.

Equations: Equations should be distinctly typed using Microsoft equation. Avoid powers of "e" and use "exp". Equations should be numbered consecutively by Arabic numerals in parenthesis at the right margin. In the text, such equation should be cited as Equation (1) etc.

Units and symbols: Symbols, units and nomenclature should conform to the recommendations of the International Union of Pure Applied Chemistry (IUPAC). SI units should be used for physical quantities.

Peer-Review: All submitted manuscripts are subjected to a peer- review process and galley proofs will be sent to the first or corresponding author where necessary.

SUBMISSION OF MANUSCRIPTS

A Processing Fee of N10,000.00 only is payable per article. All submitted articles MUST be accompanied with scanned Bank (detail below) Tellers or On-line transfer receipt as evidence of payment. Send your article(s) and Bank Teller to: njmse@msn.ng; NJMSE.msn@gmail.com. All submission of manuscripts must be sent on-line to fast-track processing and simplify the refereeing process.

PAGE CHARGE

Corresponding Authors of accepted articles will be required to pay a sum of N10,000.00 only as processing fee (at the point of acknowledging receipt of manuscript) and N10,000.00 (non-members and non-financial members of MSN), N5,000.00 (financial members of MSN) after acceptance (or $100.00 USD for processing and acceptance for other countries). They will receive free ecopy of the NJMSE volume in .pdf version. The ecopy is available online at http://njmse.msn.ng and can be downloaded free. However, printed copy(ies) may be requested for extra payment.

COPY RIGHT

Submission of an article for publication implies the transfer of the copyright of the manuscript from the author(s) to the publisher upon acceptance and that the manuscript has not been previously published elsewhere. This is the responsibility of the authors. Accepted papers become the permanent property of the publisher and may not be reproduced by any means without the written consent of the Editor-in-Chief.

Account Details: GTB PLC A/C No. 0171794514. Materials Science and Technology Society of Nigeria.

All Correspondence to:

Prof. A. Giwa
NJMSE Managing Editor
Department of Polymer and Textile Engineering
Ahmadu Bello University
Zaria. Nigeria. +2348037033052; +2348025672474
giwafat2002@yahoo.com.

Engr. Adetunji Ogunkoya
NJMSE Desk /Processing Officer,
Engineering Materials Development Institute (EMDI)
Ondo Road, PMB 611,
Akure Nigeria. +2348062207420;+2347081019516

http://njmse.msn.ng/
Emails: njmse@msn.ng; njmse.msn@gmail.com; njmsemanagingeditor@msn.ng;
editorinchief@msn.ng; njmse.editor.in.Chief@gmail.com;

Page No

TABLE OF CONTENT

Impedance and Modulus Spectroscopy of Nanocrystallite Barium Titanate Ceramic Using Mechanochemical Method.

[*]**Muazu** Alhassan, [1]**Ahmadu** Umaru, [2]**Auwalu** Inusa A., [3]**Zangina** Tasiu, **Nura** Abdullahi and [3]**Maharaz** M. Nasir

Department of Physics, Federal College of Education (T), Bichi, Kano State, Nigeria.
[1]Department of Physics, Federal University of Technology, Minna, Nigeria
[2]Department of Physics, Kano University of Science and Technology, Wudil, Kano State, Nigeria
[3]Department of Physics, Federal University Dutse, Dutse, Jigawa State, Nigeria.

[*]Corresponding authors: Email: hasumm@yahoo.com,

Abstract

Nanocrystalline $BaTiO_3$ (BT) powder was synthesized by a combination of the solid-state and mechanochemical method. X-ray diffraction, field emission scanning electron microscopy, and impedance spectroscopy utilised appropriately to characterize the BT sample (ceramic). The X-ray diffraction confirmed a single-phase perovskite compound of cubic symmetry with space group *Pm-3m*. The crystallite size and crystal cell volumes were found to be 25.7 nm and 64.250 $Å^3$ respectively. The average grain size estimated from FE-SEM was found to be 144.5 nm by using intercept technique. Electrical parameters like impedance, modulus, and electrical conductivity of the ceramic were obtained from AC complex impedance spectroscopy technique in the frequency and temperature range of 40Hz – 1MHz and 30 to 150°C, respectively. Both impedance and modulus plots showed the negative temperature coefficient of resistance (NTCR) character in the sample at 70, 110, 130, and 150°C with are similar to a semiconductor. This can be used for the fabrication of highly sensitive thermistors. The Cole-Cole (Nyquist) plot represents the grain and grain boundary conduction which indicates the ideal non-Debye type dielectric relaxation. The modulus analysis suggested the temperature-dependent relaxation process in the BT ceramic. A positive temperature coefficient of resistance (PTCR) character was observed at 90, 50, and 30°C. The activation energy values are found to be 1.12 eV and 1.07 eV for *Z''*, and M'' while it's 0.46 eV and 0.12 eV for τ_g and τ_{gb} respectively. A possible suggestion that the carrier transport is due to hopping conduction. The AC and DC conductivity spectra were found to rise with increasing temperature and frequency obey the Jonscher's power law. The conduction process was observed to be thermally activated and followed by Arrhenius law.

Keywords: Keyword: Barium titanate, Nanocrystalline, Impedance spectroscopy, AC conductivity

INTRODUCTION

Barium titanate (BT) compounds are a standout amongst other perovskite ferroelectric compounds. Broadly, in all ferroelectrics, the associated physical properties and nature of conductivity are recognized by the study of electrical conductivity. In some previous studies (Jaffe 1971; Haertling 1999; Wei and Yao 2007; Hoshina *et al.* 2008), it was found that the interior defects like A-site and oxygen vacancies typically have excellent effect on ferroelectric fatigue or ionic conductivity of the material. In view of the fact that the solid defects play vital role in the thorough applications, it is pertinent for us to acquire a primal intellect of their conductive mechanism.

One of the tools of interest is Complex impedance spectroscopy (CIS) (Macdonald 1987). It is a nondestructive method accustomed to break the grain boundary and grain-electrode effects, which conventionally remain the places of a trap for oxygen vacancies and other flaws. It is also utilized in fixing space charge polarization and its relaxation mechanism, by properly assigning different practical values of resistance and capacitance to the electro-active regions (grain and grain boundary). It typically comes to moves into the shape of complex planes as successive semicircles as observed by (Bidault *et al.* 1994; Li *et al.* 2006; Khan *et al.* 2013). The semicircles symbolised the electric phenomena involved within the polycrystalline material allegedly owing to grain, grain boundaries, electrical interface effect, and correlate between the dielectric and electrical characteristics. The complex electric modulus formalism has been utilised within the analysis of the electrical properties because it typically offers the first direct response of the majority of the used sample, abolishing the results owing to the electrode and electrical contacts. To be specific, it's peculiarly fitted to carefully extract data owing to the electrodes and ascertaining conductivity relaxation times (Hannachi *et al.*2010).

Both complex impedance and modulus spectroscopy are gainfully employed during this scholarly work because *Z''* vs *Z*' and M'' vs M' plots highlight develop the phenomenon of most massive resistance and littlest capacitance, respectively (Jacob *et al.* 2015). In this paper, we reported a comprehensive study of the conduction mechanism in nanocrystalline Barium titanate ceramic.

EXPERIMENTAL PROCEDURES

$BaTiO_3$ nanocrystalline ceramics were synthesised by a combination of solid-state reaction and high energy ball milling technique (HBM). The respective masses of the starting powders $BaCO_3$ and TiO_2 were weighed according to nominal composition using a digital

analytical balance with an accuracy of ±0.0001 g. The overall balance equation is given in Equation 1.

$$BaCO_3 + TiO_2 \rightarrow BaTiO_3 + CO_2 \quad (1)$$

A Stoichiometric amount of the weighed oxides ($BaCO_3$ and TiO_2) were mixed in an agate mortar and then ground using a pestle to obtain a first step homogeneous small particle size. The mixture plus zirconia balls were placed in a plastic jar and ball-milled for 12 h at 120 rpm using Isopropyl alcohol as a mixing agent. The weight ratio of the zirconia balls to the oxide powders was 10:1 for better milling which produced homogeneous powder of fine particles. After the mixing process, the mixture was put in a petri dish and placed in an oven and then dried at 90°C for 12 h. The dried powder was grounded again using pestle and mortar to break the caking and produced fine powder for calcination. The mixed powders of $BaCO_3$ and TiO_2 were placed in a high-temperature ceramic boat (crucible). The loaded ceramic boat was then placed in Carbolite furnace (Vecstar Ltd, U. K) and calcined at 1050°C in the air. The calcined sample and isopropyl alcohol as wetting media were put in SPEX 8000 mixer/miller machine and grind for 7 h. The milling was stopped for 15 min after every 60 minutes of milling to cool down the system. After the grinding process, the mixture (slurry) was put in a 1330 GX multipurpose oven (Sheldon manufacturing, Inc. U. S. A), and dried at 90°C for 12 h. The dried powder of the sample was compacted at 5 tons into pellet of 15 mm diameter using 5 wt% polyvinyl alcohol (PVC) as a binder. The pellets of BT sample were placed in alumina crucibles and sintered in a programmable Carbolite furnace (Vecstar Ltd, U. K) at temperatures of 1190°C for 2 h.

The phase identification of sintered BT sample was carried out using an X-ray diffractometer with monochromatic CuKα radiation (λ = 1.54178 Å) under 40 kV/30 mA over a 2θ range 20° to 80° at a scanning rate of 0.01° for 0.10 sec at room temperature (Phillips XPERT-PRO diffractometer model 7602 EA Almelo). The morphology of the BT sample is studied by Field Emission Scanning Electron Microscope (FE-SEM) using FE-SEM (JEOL-7600F) operated at 15 kV.

For electrical measurement, the BT pellets were coated with silver paint on the upper and bottom surfaces and fired at 550°C for 30 min. Impedance measurements were made over the frequency range of 40Hz - 1MHz in the temperature range of 30-150°C, using Agilent A 4294 Impedance Analyzer. An applied voltage of 100 mV is used. The famous software package EC-Lab version 1040 has been employed to analyse the impedance spectroscopy (IS) data based on equivalent circuits.

RESULT AND DISCUSSION

X-ray Diffraction

BT ceramic X-ray diffraction pattern taken at room temperature is shown in Figure 1(a). A single-phase perovskite structure is seen lacking any visible trace of impurity within the background. The magnified XRD pattern in the range of 2θ from 44.5 to 46.0° (Figure 1(b)) illustrated that the crystal structure of BT was assigned to the cubic phase with Pm-3m space group verified from JCPDS database (card no 96-150-7758), since the (200)/ (002) peaks are unseparated (Buttner and Maslen 1992; Veselinovic *et al.* 2014) as reported by other researchers (Lazarevi *et al.* 2010; Itasaka *et al.,* 2018).

The lattice constant of the sample was calculated using the Equation 2

$$a^2 = \frac{\lambda}{2}\frac{[(h^2+k^2+l^2)]}{\sin^2\theta} \quad (2)$$

and the Debye Scherrer equation for calculating the crystal size is given by (Scherrer 1918).

$$D = \frac{0.98\lambda}{\beta \cos\theta} \quad (3)$$

where λ is the wavelength of the x-ray (λ = 1·54178 Å), θ is the Bragg angle and hkl are the Miller indices of the corresponding planes, D is the crystallite size, 0.98 is the crystallite shape factor and β is the full width at half maxima (FWHM) at Bragg's angle (2θ).

The lattice parameters, crystallite size, and unit cell volume of BT ceramic sintered at 1190°C for 2 h were estimated. The lattice parameters and unit cell volume of BT were found to be $a = b = c = 4.00522$ Å and 64.250 $Å^3$ respectively. The crystallite size of BT was calculated using equation 2 is found to be 25.7 nm and is similar to the one obtained by other researchers (Al-Naboulsi *et al*. 2016; Yun *et al*. 2019).

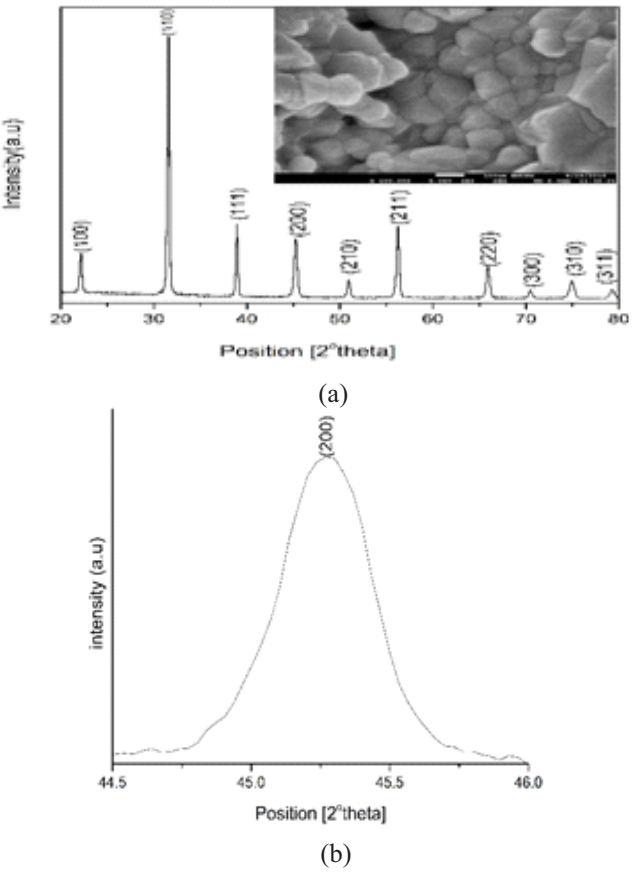

Figure 1: (a) Room Temperature XRD Patterns and inset FESEM Micrograph at x200,000 Magnification for BT Ceramic; (b) Enlarged XRD Patterns from 44.5 to 46.0° of BT Sintered at 1190°C

Surface Morphology

The inset of Figure 1(a) shows the FESEM micrograph of BT ceramics sintered at 1190°C for 2 hrs. It can be sighted that the sintered ceramic sample is dense with the presence of voids and varying microstructures. The appearance of voids in the FESEM image revealed the presence of pores in the sample, an indication of particle agglomeration. The grain size and boundary were observed clearly in non-agglomerated regions while the shape of the grains was indistinguishable. The average grain size of BT ceramic obtained by using the intercept technique (Abrams 1971) was found to be 144.5 nm.

Complex Impedance Spectroscopy

Figure 2(a) and 2(b) show the observed variation of real *Z'* and imaginary *Z''* part of complex impedance with a frequency of BT ceramic at a temperature range of 30-150°C. At a temperature of 30, 50, 90°C, and 70, 110, 130, 150°C a monotonous decrease of *Z'* is seen with increasing frequency which became almost frequency-independent above ~100 Hz and 1000 Hz respectively. It may reasonably be due to the possible release of space charges as a potential consequence of a decrease in the barrier properties of BT ceramics with increased temperatures as inferred by (Biswal *et al.* 2014; Mandal *et al.* 2016). An observed increase of *Z'* at temperature of 30, 50, and 90°C indicated lower conductivity and polarization of the material at temperature. Figure 2(b) shows a decreasing *Z'* with increasing frequencies up to ~1000 Hz above which it merged seamlessly at a higher frequency. The observed value of *Z''* increases at low-frequency at a temperature of 70, 110, 130, and 150°C reached the maxima (Z'_{max}) at an elevated temperature of 110, 130, and 150°C. The Z'_{max} shifted to higher frequencies with increasing temperature with the presence of relaxation (peaks) at these temperatures. This amply demonstrates the non-Debye nature in the material (Kumar *et al.* 2014).

Conversely, *Z''* was discovered to decrease monotonously with increasing frequency and decreasing temperatures of 90, 50, and 30°C. This demonstrated that the material exhibited a positive temperature coefficient of resistivity (PTRC) (Kumari, *et al*. 2016). The maximum and minimum values of *Z'* were 33.3 MΩ, and 0.93 MΩ, while values of *Z''* were 22.8 MΩ, and 3.00 MΩ respectively. The maximum and minimum values of *Z'* were 33.3 MΩ and 0.93 MΩ, while values of *Z''* were 22.8 MΩ and 3.00 MΩ respectively.

The likeliest value of the relaxation frequency was
d using the relation

$$2\pi f_{max} C = (2\pi f_{max})\tau = 1 \quad (4)$$

e $\tau = RC$ is the the likeliest relaxation time
apanda *et* $\tau = \tau_o \exp\left(\frac{\Delta E_a}{K_B T}\right)$ st likely relaxing
is in line s law given by

(5)

e τ_o is the relaxation time at a pro exponential
r, Is a constant associated with the charge carrier
ity. By using Equation 4, the activation energy (E_a)
aluated.

Figure 3 shows the variation of normalized
meters of Z''/Z''_{max} as a function of logarithmic
alized frequency f/f_{max} and Arrhenius plot of log

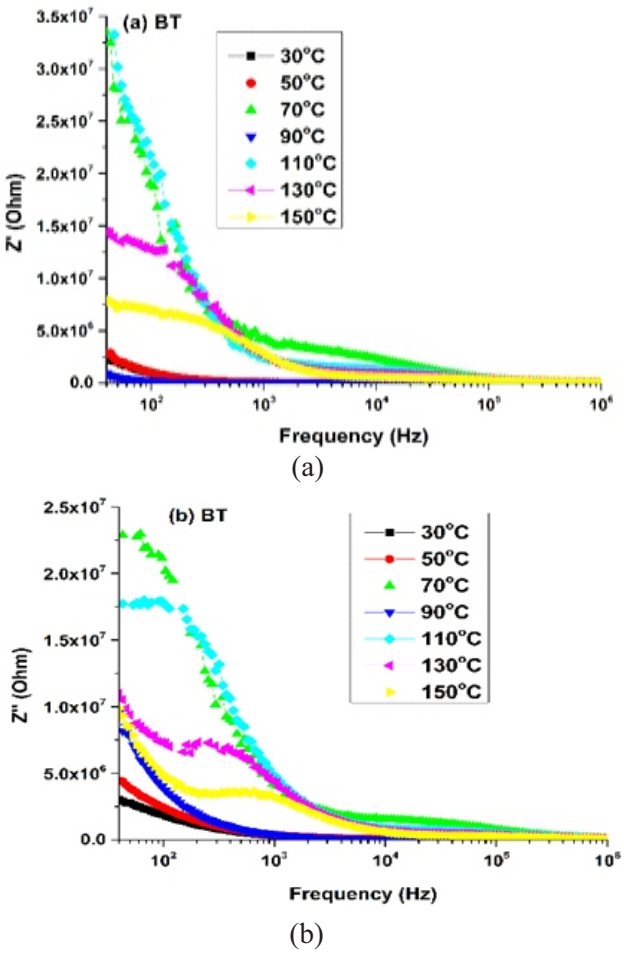

Figure 2: Variation of (a) Real (*Z'*) and (b) Imaginary (Z'') with Frequency for BT Ceramic

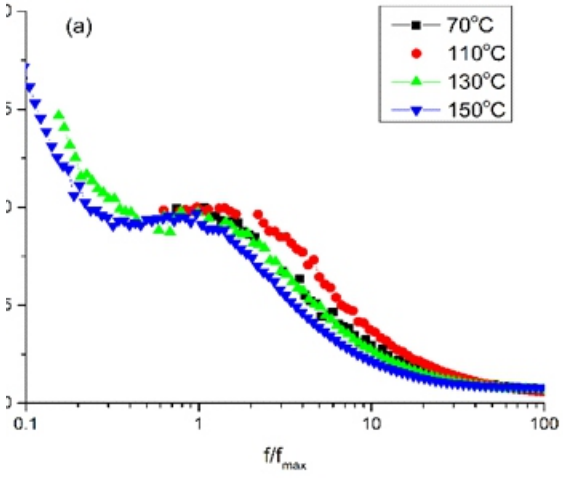

Figure 3: Normalized Parameter of Z''/Z''_{max} versus log (f/f_{max}) Plots at various Temperatures.

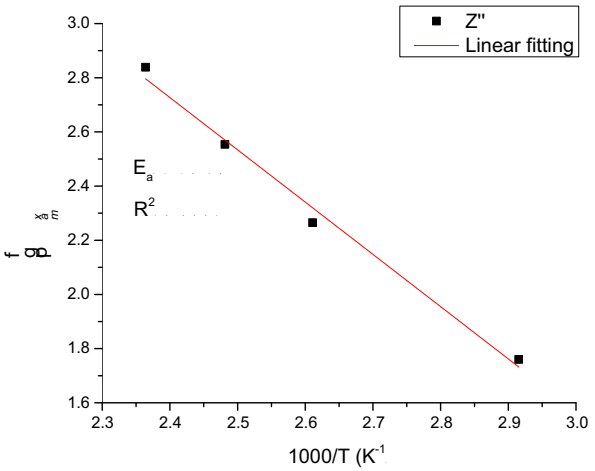

Figure 4: Arrhenius Plot of log (f_{max}) versus 1000/T for BT Ceramic.

versus 1000/T. In this figure, it can be observed that different peaks nearly coalesce at the same peak irrespective of the temperature. The overlapping of peaks showed relaxation time was temperature independent suggesting the presence of long-range and localized system relaxations. For a localized electron to be mobilised, the support of lattice vibrations was indispensable. For such specific cases, mobile electrons were regarded not to move by vibration, but by hopping motion actuated by vibration from the lattice. Figure 4 presents the Arrhenius plot drawn between log(f_{max}) versus 1000/T found from *Z*" plot. The activation energy (E_a) determined from the linear fit was found to be 1.12 eV for Z".

The importance of Nyquist (Cole-Cole) plot is to examine the relaxation and conduction procedures. This was useful in the determination of various criteria relating to the effects of grain and grain boundaries. Figure 5(a) and 5(b) shows the Nyquist (Cole-Cole) plot of imaginary *Z*" against the real *Z*' at various temperatures. At temperature of 30°C, 50°C, and 90°C, it was observed that the line gradient decreased with a decrease of temperature, and the curve proceeded towards the real *Z*' axis indicating reduced sample conductivity. This showed evidence of a positive temperature coefficient of resistance (PTCR) effect at the temperature of 30°C, 50°C and 90°C. At temperature of 70, and 110-150°C two depressed semicircles symbolizing both the grain and grain boundaries were discovered.

The high and low-frequency semicircle represented the tangible contribution, respectively, due to grains and the grain boundary effect. (Humera *et al.* 2020). Also, the semicircles comprised of depression, indicating that the distribution of relaxation times remains a non-Debye type. This was due to grain orientation, grain boundary, stress-strain phenomenon, and distribution of atomic defects (Sen *et al.* 2007). To find the parameters concerning grains and grain boundaries, experimental data adhere to an analogous circuit comprising two parallel resistance-capacitance (RC) elements or

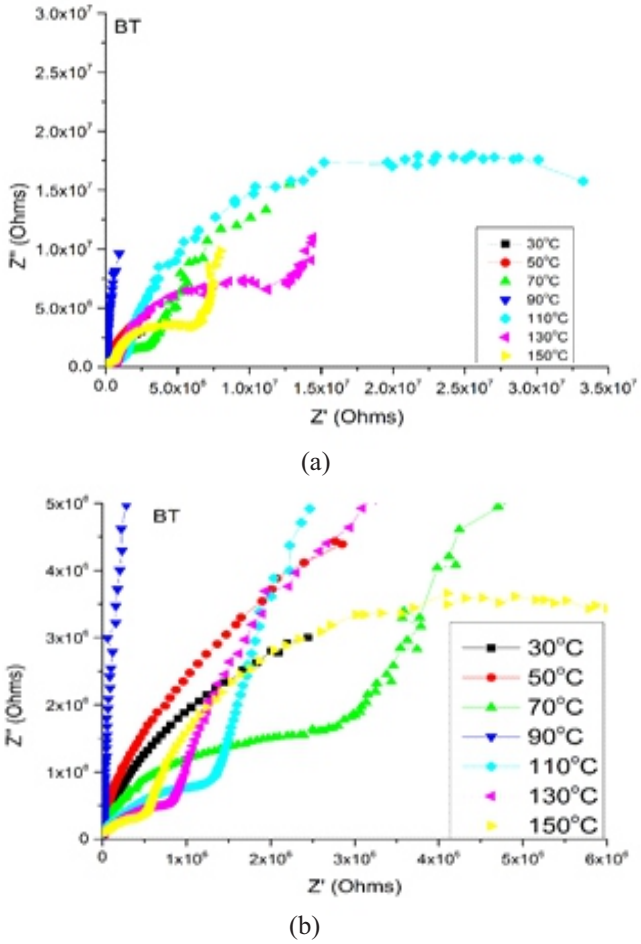

Figure 5: (a) Variation of *Z''* with *Z'* (Nyquist or Cole-Cole) Plot for BT Ceramic.(b) when (*Enlarged*).

replacing the capacitor with a constant phase element (CPE) as a parallel-connected resistance-constant phase element (*R-CPE*) network (Mondal *et al.* 2017). The Constant phase element (CPE, denoted by Q) was used to overcome dispersion and non-linearity in the value from ideal behavior or because the semicircles exhibit a non-Debye nature. It is defined as $C = (R^{1-n} Q)^{1/n}$ where *n* represents the degree of deviation with respect to the value of the pure capacitor. It is zero (0) and unity (1) for an ideal resistor and capacitor respectively (Barick *et al.* 2013). The circuit fitting parameter was performed using EC-Lab Software V10.40 with the modeled circuits as shown in Figure 6. Table 1 provides the fitting parameters for the equivalent circuit (R-CPE). The relaxation time for the grain (τ_g) and grain boundary τ_{gb} was calculated from Equation 4. It was observed that the values of grain resistance (R_g) decreased with an increasing temperature this indicated an increase of conductivity with rising temperature.

Complex Dielectric Modulus

Modulus analysis typically represents an alternative method for properly examining the material's electrical properties and improving the various impacts present in the ceramic to specific time constants for relaxation. The real (*M*') and imaginary (*M*") parts of the modulus are calculated using Equations 6 and 7:

Table 1: Parameters Obtained from Temperature Dependent Impedance Spectroscopy Data for the BT Ceramic.

Temp. (°C)	$R_g \times 10^6$ (Ω)	$Q \times 10^{-12}$ (F)	n_1	$R_{gb} \times 10^6$ (Ω)	$Q_2 \times 10^{-12}$ (F)	n_2	$\tau_g \times 10^{-6}$ (s)	$\tau_{gb} \times 10^{-3}$ (s)
70	2.96	5.16	0.92	7.38	2.03	0.79	5.52	4.86
110	1.98	33.1	0.79	3.69	26.8	1.0	5.73	0.99
130	1.01	23.9	0.83	1.32	29.7	0.99	2.75	5.36
150	0.64	63.1	0.77	0.70	37.7	0.97	2.00	2.89

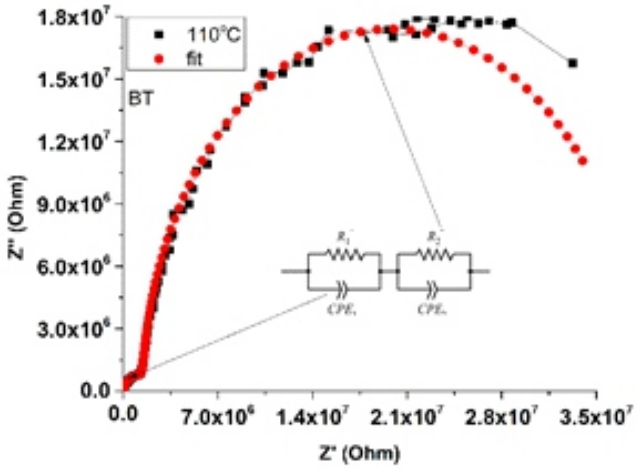

Figure 6. The Model of an Equivalent Circuit used for Fitting of Impedance Spectra

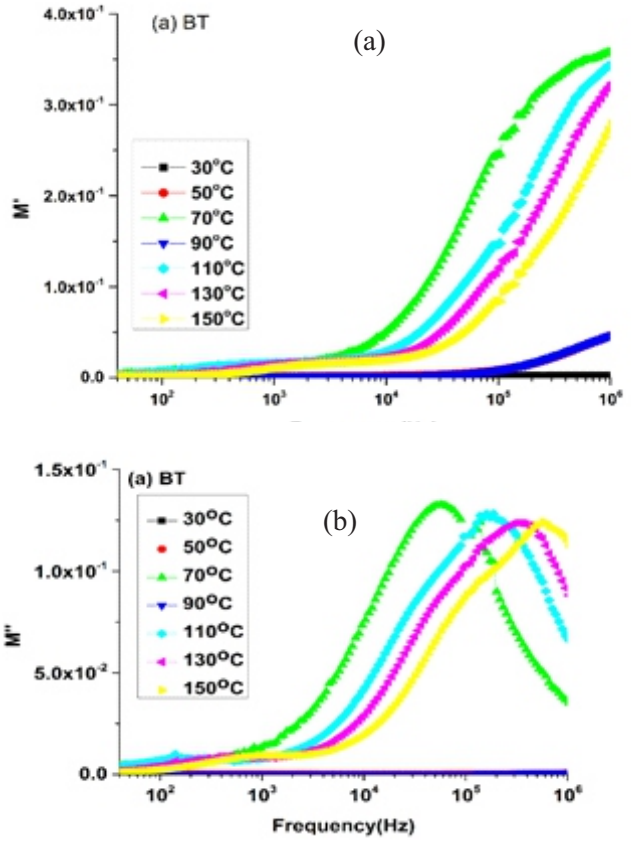

Figure 7: Frequency-temperature Dependence of (a) Real Part (*M'*) and (b) Imaginary Part (*M''*) for BT Ceramic.

$$M' = \frac{\varepsilon'}{\varepsilon'^2 + \varepsilon''^2} \quad (6)$$

$$M'' = \frac{\varepsilon''}{\varepsilon'^2 + \varepsilon''^2} \quad (7)$$

Figure 7(a) and 7(b) show the real (*M'*) and imaginary (*M''*) frequency dependence parts of electrical modulus at 30-150°C. It was noticed that the *M'* value at lower frequencies is almost zero, affirming the presence of a significant electrode and/or ionic polarization in the temperature ranges examined. The *M'* value increased continuously with increasing frequency and the dispersion changes to a higher frequency towards a high-frequency limit. This merely occurred because of the presence of the conduction procedure owing to the short-range mobility of the carriers in charge.

It can be observed from Figure 7(b) that *M''* values increased with increasing frequency and temperature. It reached a maximum (M''_{max}) with the appearance of impedance relaxation peaks which appeared at 70°C, 110°C, 130°C, and 150°C at frequencies below 10^4 Hz. At that point, *M''* started to decrease with an increasing frequency above the maxima. For rising temperatures, the peaks shifted to a higher-frequency side. This means the relaxation processes are temperature-dependent in these materials. The intensity of this peak decreased slowly because the impedance values decreased with temperature rise. The asymmetric module peaks change to a higher frequency side revealing the association of mobile ion movements (Jacob *et al.* 2015; Sharma *et al.* 2015). The broadening of the peaks is because of the spread of relaxation time with the different time constants (Mondal *et al.* 2017) and so relaxation was of a non-Debye type. The area below and above the relaxation peaks in *M''* defined the field where the load carrier can travel for both long and short distances (Naidu *et al.* 2018). The difference in the charging carriers indicates a hopping mechanism makes the electrical conductivity important at a higher temperature. At a temperature of 30, 50, and 90°C the value of *M''* appeared to become independent of both the frequency and temperature. It presented a possible release of space charge.

Figures 8 shows the modulus scaling behavior by plotting normalized parameters and the Arrhenius relation of BT ceramic. The scaling action of the modulus provided an insight into the dielectric processes within the material (Das *et al.* 2007). In Figure 8 it was observed that the peaks overlapped at 70-130°C, suggesting temperature-independent behavior of the complex processes in the ceramics (Saha and Sinha

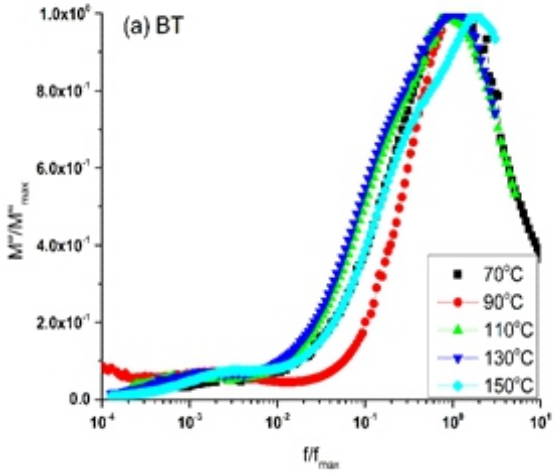

Figure 8: Normalized parameters M''/M''_{max} versus $\log (f/f_{max})$

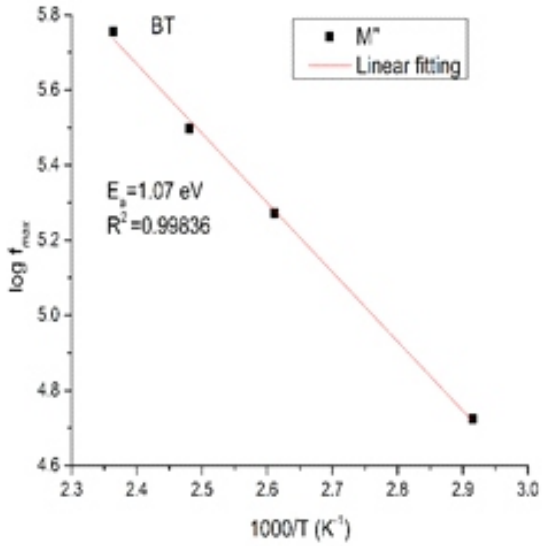

Figure 9: Arrhenius plot of $\log (f_{max})$ versus 1000/T for BT ceramic.

2002). The peak that appeared at 150°C shifted towards a higher frequency side, activating another relaxation process. The dielectric analysis of material can, therefore, be investigated by means of modulus scaling (Das *et al.* 2007). Figure 9 shows the Arrhenius plot of $\log (f_{max})$ versus 1000/T found from *M*'. The activation energy obtained from the slope of the straight line was found to be 1.07 eV which was close to the activation energy value found from *Z*" in Figure 4.

Figure 10 shows the Arrhenius plot of ln τ_g and ln τ_{gb} with the inverse of absolute temperature (1000/T) for BT ceramic. The activation energies for relaxation were calculated from Equation 8 to be 0.46 and 0.12 eV for grain and grain boundary respectively.

The temperature dependence of the complex modulus spectrum (i.e. *M*' vs *M*") spectrum of BT ceramic at 30-150°C is shown in Figure 11. At a temperature of 70°C, 110, 130, and 150°C two semicircular arcs in low and high frequencies regions were observed. Low and high-frequency small and wide semicircular arcs are due to poor

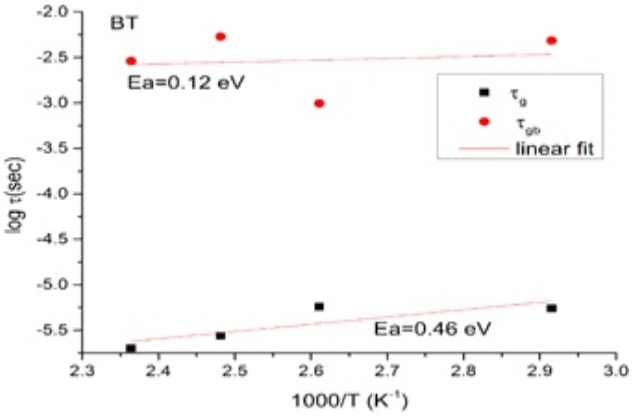

Figure 10: Arrhenius Plot of ln τ_g and ln τ_{gb} versus 1000/T for BT Ceramic.

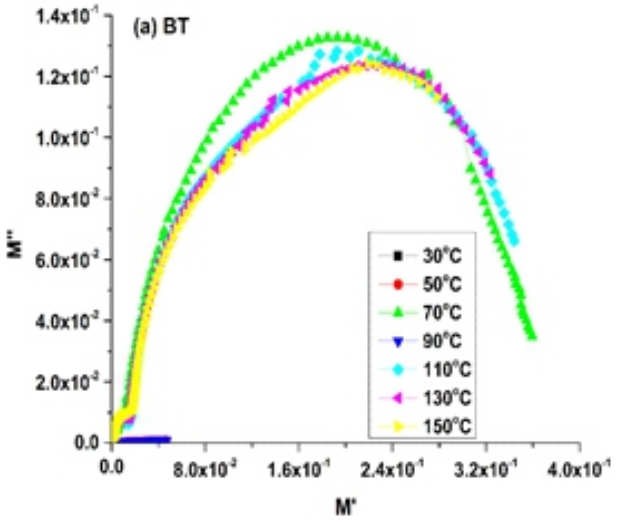

Figure 11: Plot of *M*' versus *M'* for BT Ceramic.

grain boundary effects rather than dominant grain effects and bulk or grain reaction, respectively (Lvovich 2012; Saghrouni *et al,* 2014). The relaxation in the material was non-Debye form as the semicircular arc centers are below the actual M' axis. It appeared that the intercept of the semicircles on the real axis tend to change with increasing temperature to higher values of *M*'. It showed that capacitance increased with increasing temperature. This affirmed the NTCR type behavior of the BT ceramic since the capacitance of bulk (C_b) was inversely proportional to the resistance of bulk (R_b)

AC Conductivity Analysis

The AC conductivity (σ_{ac}) was computed using Equation 8.

$$\sigma_{ac} = \omega\varepsilon'\varepsilon_o \tan\delta \qquad (8)$$

where $\omega = 2\pi f$, f is the frequency, ε' the real dielectric constant, ε_o permittivity of free space and tan δ is the loss tangent.

The plot of log σ_{ac} vs log f at different temperatures is shown in Figure 12. It depicted wide dispersion and the conductivity increased as temperature increased with three clearly distinguishable areas in the conducting

regions. However, at high-frequency, the conductivity exhibits frequency dispersion. The AC conductivity increased with a frequency and temperature rise similar to the behavior observed in many of the polymers and semiconductors (Dutta *et al.* 2008). This is due to the change in the mobility of the sample charging carriers as the temperature increased. In the high-frequency field, however, the conductivity showed dispersion with an increasing slope for all the temperatures. The frequency at which the slope changed is known as the frequency of hopping which shifted with an increasing temperature towards the higher values. The power-law equation expressed the total conductivity (σ) of a given material at a given temperature (Jonscher 1996),

$$\sigma_{ac} = \sigma_{dc} + A\omega'' \quad (9)$$

where σ_{dc} is the extrapolated conductivity value of the frequency (at $\omega = 0$). independent part, and A is the AC coefficient, n ($0 \leq n \leq 1$) the correlation exponent of the ions. Thermally activated quantities are typically given as A and n, therefore, electrical conduction remained a thermally activated operation. As Jonscher stated, the possible source of frequency dependence on conductivity lies within the relaxation phenomena that arose from mobile charging carriers.

Figure 13 shows the Arrhenius plot of AC and DC

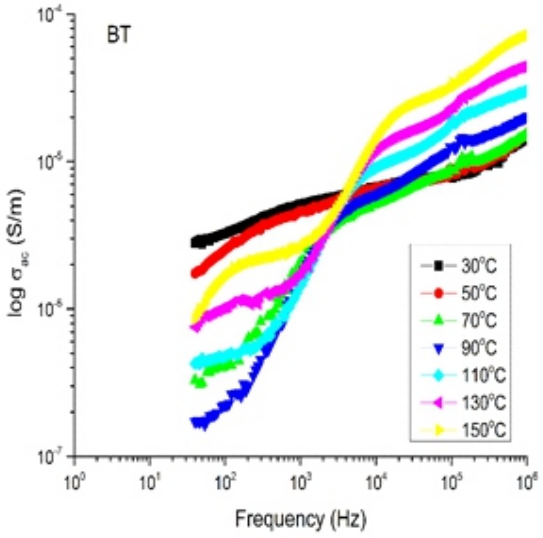

Figure 12: Variation of AC Conductivity with Frequency for BT Ceramic.

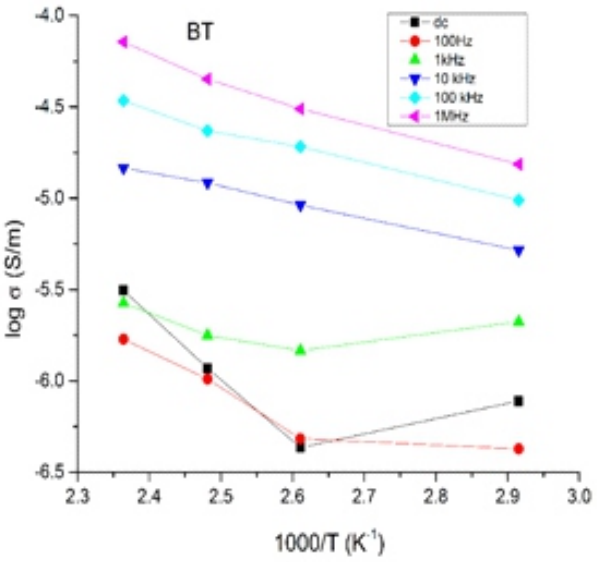

Figure 13: Variation of AC Conductivity with an Inverse Absolute Temperature at Various Frequencies

conductivity versus inverse temperature of BT ceramic. It was observed that the conductivity of the high-temperature component which can be related to the bound charge carriers in the ceramics increased. On top of that, it was observed that the slopes of AC conductivity at a frequency of 100 Hz, 1 kHz, and DC conductivity were not linear but showed little alterations at different temperature regions. This may be attributed to contributions from various areas, like grain and grain boundary (Mahboob *et al.* 2006). The AC and DC conductivity activation energies were carefully determined with the following formula:

$$\sigma_{ac} = \sigma_o \exp\left(\frac{-E_{ac}}{k_B T}\right) \quad (10)$$

$$\sigma_{dc} = \sigma_o \exp\left(\frac{-E_{dc}}{k_B T}\right) \quad (11)$$

whence

$$\ln \sigma_{dc\ or\ ac} = \ln \sigma_o \quad (12)$$

where σ_o is pre-exponential factor, k is Boltzmann constant, T is the absolute temperature, E_{ac} and E_{dc} represent activation energy of AC and DC conductivity, respectively.

The apparent activation energy E_a is obtained from the linear lowest-square fit slope of the conductivity data in Equation 5, and the result is shown in Table 2. At higher temperature ranges, the activation energies DC and AC (100 and 1 kHz) were greater than those at lower

Table 2: The AC and DC conductivity activation energies (eV) for BT ceramic.

Sample	BT					
	Conductivity Activation Energy (eV)					
		AC				
Temperature (°C)	DC	100 kHz	1 kHz	10 kHz	100 kHz	1 MHz
70-150	-	-	-	0.48	0.56	0.68
70-110	0.48	0.10	0.30	-	-	-
130-150	2.02	1.28	0.60	-	-	-

temperature ranges. The E_a values 1 kHz and 1 MHz were in agreement with the earlier report (Humera *et al.* 2020; Tomar *et al.* 2020). Accordingly, the calculation of activation energy was based on the considerable degree of ionization of the oxygen vacancy (Moretti and Michel, 1987). Activation energy > 1.0 eV related to single ionized vacancies (Ang *et al.,* 2000) and/or electronic mobility in space charge regions (Ortega *et al.* 2007). In this manner, the conduction cycle within this temperature range could be due to the BT ceramic's hopping of charge carriers and or individually ionized oxygen vacancies (Badapanda *et al.* 2014). In perovskite ferroelectric, oxygen vacancies are typically regarded as one of the mobile charging carriers and so the ionization of oxygen vacancies produced electrons for conduction.

CONCLUSION

A combination of solid-state and high energy ball milling technique has been used to synthesise nanocrystalline $BaTiO_3$ powder. A single-phase perovskite cubic was observed at room temperature from the XRD pattern. FE-SEM image showed that sample was dense and had different microstructures with a certain amount of porosity. Both impedance and modulus analysis at 70, 110, 130 and 150^{o}C supported the typical behavior of a negative temperature coefficient of resistance (NTCR) of the materials which would be effective for the fabrication of a highly sensitive thermistor and suggested the relaxation to be non-Debye type. Conversely, at a temperature of 30, 50, and 90^{o}C the material showed a PTCR effect. The activation energy values suggested the carrier transport was due to hopping conduction. The AC conductivity was found to obey the universal power law, as hinted by Jonscher. The magnitude of the activation energy followed the Arrhenius relationship.

ACKNOWLEDGMENT

The authors gratefully acknowledge the Physics Department, Faculty of Science, UPM, Malaysia for providing support and facilities to carry out structural and electrical measurements. Thanks also go to my supervisor Prof. Dr. Abdul Halim Shaari for helpful suggestions and many valuable discussions.

REFERENCES

Abrams, H. (1971). Grain Size Measurement by the Intercept Method. *Metallography,* 4(1):59-78. https://doi.org/10.1016/0026-0800(71)90005-X

Al-Naboulsi, T., Madona, B., Christophe, T., Pascal, D., Zakhour, M., Sophie, G.F. (2016). Elaboration and Characterization of Barium Titanate Powders Obtained by the Mechanical Activation of Barium Nitrate and Titanate Oxide, and Electrical Properties of the Ceramics Sintered by SPS. *Journal of Ceramic Processing Research,* 17(8):870-875.

Ang, C., Yu, Z., and Cross, L.E. (2000). Oxygen-Vacancy-Related Low-frequency Dielectric Relaxation and Electrical Conduction in Bi: $SrTiO_3$. *Physical Review B*, 62:228-23.

Badapanda, T., Harichandan, R.K., Nayak, S.S., Mishra, A., and Anwar, S. (2014). Ferroelectric Relaxor Behavior in Hafnium Doped Barium-titanate Ceramic. *Processing Application of Ceramics*, 8(3):145–153.

Barick, B.K., Choudhary, R.N.P., Pradhan, D.K. (2013). Dielectric and Impedance Spectroscopy Of Zirconium Modified $(Na_{0.5}Bi_{0.5})TiO_3$ Ceramics. *Ceramic. Int*., 39:5695–5704.

Bhargavi, G. N., Khare, A., Badapanda, T., M. Anwar, M.S. and Brahme, N. (2017). Electrical Characterizations of $BaZr_{0.05}Ti_{0.95}O_3$ Perovskite Ceramic by Impedance Spectroscopy, Electric Modulus And Conductivity, *Journal of Materials Science: Materials in Electronics,* 28:16956–16964

Bidault, O., Goux, P., Kchikech, M., Belkaoumi, M., and Maglione, M. (1994). Space-charge Relaxation in Perovskites. , *Physical Review B*. 49:7868.

Biswal, M. R., Nanda, J., Mishra, N. C., Anwar, S. A. Mishra, A. (2014). Dielectric and Impedance Spectroscopic Studies of Multiferroic $BiFe_{1-x}NixO_3$, *Advance Material Letters,* 5(9): 531-537

Buttner, H. R. and Maslen, E. N. (1992). Structural Parameters and Electron Difference Density in $BaTiO_3$. *Acta Crystallographica B*, 48:764 - 769,

Das, P.S., Chakraborty, P.K., Behera, B., and Choudhary, R.N.P. (2007). Electrical properties of $Li_2BiV_5O_{15}$ ceramics. *Physica B*, 395:98–103.

Hannachi, N. I., Chaabane, K., Guidara, A., and Bulou, F. H. (2010). AC Electrical Properties and Dielectric Relaxation of $[N(C_3H_7)_4]_2Cd_2Cl_6$, single crystal. *Material Science and Engineering, B* 172:24-32

Haertling, G. H., (1999). Ferroelectric ceramics: history and technology. *Journal of American Ceramic Society,* 82 (4):797-818.

Hoshina, T., Takizawa, K., Li, J., Kasama, T., Kakemoto H., and Tsurumi, T. (2008). Size Effect of Barium Titanate: Fine Particles and Ceramics. *Japan Journal Applied Physics*, 47:7607-7611.

Humera, N., Riaz, S., Ahmad, N., Arshad, F., Zafar, R., Ali, S., Idrees, S., Noor, H., Atiq, S., and Naseem, S. (2020). Colossal Dielectric Constant and Ferroelectric Investigation of $BaTio_3$ Nano-ceramics, *Journal of Materials Science: Materials in Electronics,* 31:5420-5415

Itasaka, H., Mimura, K.I. and Kato, K. (2018). Extra Surfactant-Assisted Self-Assembly of Highly Ordered Monolayers of $BaTiO_3$ Nanocubes at the Air–Water Interface, *Nanomaterials* 8(9):739; doi:10.3390/nano8090739

Jacob, R., Harikrishnan Nair, G., Isac, J. (2015). Impedance Spectroscopy and Dielectric Studies of Nanocrystallite Iron Doped Barium Strontium Titanate Ceramics. *Processing and Application of Ceramics,* 9(2):73–79.

Jaffe, B., Cook, W. and Jaffe, H. (1972). *Piezoelectric Ceramics*. Academic Press, New York: pp. 53-91.

Jonscher, A.K. (1996). *Universal Relaxation Law*. Chelsea Dielectrics Press, London.

Khan, H.M., Pal, S. and Bose, E. (2013). Room Temperature Frequency-dependent Complex Impedance and Conductivity Behavior of $BaTiO_3$–$La_{0.7}Ca_{03}MnO_3$ Composites. *Canadian Journal of Physics*, 91(12):1029-1033.

Kumari, K. Prasad, A., and Prasad, K. (2016). Dielectric, Impedance/Modulus and Conductivity Studies on $(Bi_{0.5}(Na_{1-x}K_x)_{0.5})0.94Ba_{0.06}TiO_3$, $(0.16 \leq x \leq 0.20)$ Lead-Free Ceramics. *American Journal of Materials Science,* 6(1):1-18.

Kumar, M., Shankar, S., Parkash, O. and Thakur, O.P. (2014). Dielectric and Multiferroic Properties of $0.75BiFeO_{3-0}2.5$ $BaTiO_3$ Solid Solution. *J. Mater. Sci. Mater. Electron.* 25:888–896.

Rom, M. J. Rom, N. Paunovi, N., Stojanovi, B.D. (2010). The characterization of the barium titanate ceramic powders Prepared by the Pechini type reaction route and mechanically assisted synthesis. *Journal of the European Ceramic Society,* 30:623–628.

Li, J.Y., Chen, X. M., Hou, R. Z., Tang, Y. H., (2006). Maxwell–Wagner Characterization of Dielectric Relaxation in $Ni_{0.8}Zn_{0.2}Fe_2O_4/Sr_{0.5}Ba_{0.5}Nb_2O_6$ Composite. Solid State Commun. 137(3):120-125.

Lvovich, F.V. (2012). *Impedance Spectroscopy. Applications to Electrochemical and Dielectric Phenomena,* John Wiley & Sons, Inc.

Macdonald, J.R., (1987). Ed. Impedance spectroscopy--Emphasizing solid materials and systems. New York: Wiley-Interscience.

Mahboob, S., Prasad, G., and Kumar, G.S. (2006). Electrical conduction in $(Na_{0.125}Bi_{0.125}\ Ba_{0.65}Ca_{0.1})\ (Nd_{0.065}Ti_{0.87}Nb_{0.065})O_3$ ceramic)O_3 ceramic. Material Bulletin of science, 29(1):35-41.

Mandal, S. K., Singh, S., Dey, P., Roy, J. N., Mandal, P. R. and Nath, T. K. (2016). Frequency and Temperature Dependence of Dielectric and Electrical Properties of TFe2O4 (T=Ni, Zn, Zn0.5Ni0.5) Ferrite Nanocrystals,, *Journal of Alloys and Compound*, 656:887-896.

Mondal, T., Das, S., Badapanda, T., Sinha, T.P., and Sarun, P.M. (2017). Effect of Ca^{2+} Substitution on Impedance and Electrical Conduction Mechanism of $Ba_{1-x}Ca_xZr_{0.1}Ti_{0.9}O_3$ ($0.00 \leq x \leq 0.20$) Ceramics. *Physica B: Physics of Condensed Matter*, 508:124-135

Moretti, P., Michel, C.F.M. (1987). Impurity Energy Levels And Stability of Cr and Mn Ions in Cubic $BaTiO_3$. *Physical Review B,* 36:3522-3527.

Naidu, K.C.B., Reddy, V. N., Sarmash, T. S., Kothandan, D., Subbarao, D., Kumar, N. S. (2018). Structural, Morphological, Electrical, Impedance and Ferroelectric Properties of BaO-ZnO-TiO_2 Ternary System, *Journal of the Australian Ceramic Society*, 55:201-218

Ortega, N., Kumar, A., Katiyar, R.S., and Scott, J.F. (2007). Maxwell-Wagner space charge effects on the Pb(Zr, Ti)O_3eCoFe_2O_4 multilayers. *Applied Physics Letters,* 91:102902.

Saghrouni, H., Jomni, S., Belgacem, W., Hamdaoui, H., and Beji, L. (2014). Physical and electrical characteristics of metal/Dy/2O_3/p-GaAs structure. Physica, B, 444:58-64.

Saha, S. and Sinha, T.P. (2002). Low-temperature Scaling Behavior of $BaFe_{0.5}Nb_{0.5}O_3$. *Physical. Review B*, 65:134103.

Scherer, P., (1918). Determination of the Size and Internal Structure of Colloidal Particles Using X-rays, News from the Society of Sciences, Gottingen. *Mathematical-Physical Class*, 2: 98-100.

Sen, S., Pramanik, P., and Choudhary, R.N.P. (2007). Effect of Ca-Additions on Structural and Electrical Properties of Pb(SnTi)O_3 Nano-Ceramics. *Ceramics International*, 33(4):579-587.

Sharma, S., Shamim, K., Ranjan, A., Rai, R., Kumari, P., and Sinha, S. (2015), Impedance and modulus spectroscopy characterization of lead-free barium titanate ferro-electric ceramics, Ceramics International, 41:7713-7722

Tomar. R., Pandey, R., Singh, N. B., Gupta, M. K. Gupta, P. (2020). Electrical Properties of Barium Titanate in presence of Sn^{2+} dopant. *SN Applied Sciences,* 2:226

Veselinovic, L., Mitric, M., Mancic, M., Vukomanovic, M., Hadzic, B., Markovic, S. and Uskokovic, D. (2014). The Effect of Sn for Ti Substitution on the Average and Local Crystal Structure of $BaTi_{1-x}Sn_xO_3$ ($0 \leq x \leq 0.20$). *Journal of Applied Crystallography,* 47:999-10070.

Wei, X., and Yao, X. (2007). Preparation, structure and dielectric property of barium stannate titanate ceramics. Material and Science Engineering, B 137(1-3): 184-188.

Wu, Y.T., Wang, X. F., Yu, C.L., and Li, E. Y. (2012). Preparation and Characterization of Barium Titanate ($BaTiO_3$) Nano-Powders by Pechini Sol-Gel Method. *Materials and Manufacturing Processes*, 27(12):1329-1333.

Yun, B .G., Lee, H.M., Jeong, D. Y., Lee, W. I., Cho, N. H.